CHIN. PHYS. LETT. Vol. 33, No. 4 (2016) 046101

The Magnetic Order in Ion Irradiated Graphite *

Li-Juan Li(李丽娟)[1], Xin-Mei Yang(杨新梅)[2]**, Hui-Hao Xia(夏汇浩)[2], Zhou-Tong He(贺周同)[2], Xing-Tai Zhou(周兴泰)[2], Xiang-Dong Liu(刘向东)[3]

[1]*Shandong Institute of Commerce and Technology, Jinan 250103*
[2]*Shanghai Institute of Applied Physics, Chinese Academy of Sciences, Shanghai 201800*
[3]*School of Physics, Shandong University, Jinan 250100*

(Received 10 December 2015)

The magnetism of highly oriented pyrolytic graphite (HOPG) induced by ion implantation is investigated with electron spin resonance (ESR) spectroscopy and magnetization measurements. The results indicate that the ESR spectra of the HOPG sample correlate with ion species, incident energy and dose of implantation. The correlation of the ESR spectra and magnetism of the HOPG sample with $^{12}C^{+}$ ion implantation and H^{+} ion implantation are studied in detail. The ferromagnetism of the HOPG sample is likely related to the asymmetric L1 line, which may be attributed to the interaction between localized defects and itinerant electrons occupied in the 'impurity' band induced by ion implantation.

PACS: 61.80.Jh, 76.30.−v DOI: 10.1088/0256-307X/33/4/046101

Ferromagnetism of graphite is a challenge to the traditional theory of ferromagnetism. The origin of ferromagnetic ordering in graphite has excluded the contribution of transition metal impurities.[1−3] Magnetic ordering in ion implanted graphite is observed by magnetic force microscopy (MFM).[3−7] Magnetic moment of graphite is detected by a superconducting quantum interferometer device (SQUID) magnetometer.[5,7−12] It has been revealed that 265 ppm of Fe^{+} ions can only produce paramagnetism,[13] however H^{+} ion implantation and $^{12}C^{+}$ ion implantation can produce obvious ferromagnetism with increasing the remnant magnetism.[7−12] Ferromagnetism in graphite is found to have the character of 2D magnetism.[8] The normalized saturated magnetic moment is linear decreasing with the increasing temperature, which can be interpreted with the excitation of 2D spin wave.[14,15] Studies of ferromagnetism in metal-free carbon films by soft x-ray magnetic circular dichroism (XMCD) spectra have revealed that there is clear XMCD signal only at 284.0 eV of photon energy corresponding to π electrons,[10,16] which indicates that π electrons play a significant role for the ferromagnetism of graphite. The magnetic order in graphite-like films induced by a 2.25 MeV focused proton beam was investigated with MFM, indicating that the magnetic order induced by proton irradiation is in the area surrounding the beam impact area.[3] The correlation between ferromagnetism and conductivity of proton implanted highly oriented pyrolytic graphite (HOPG) is investigated with Kelvin probe force microscopy (KPFM), predicting that there is an insulating semiconducting magnetic state[17] induced by the 2.25 MeV proton microbeam implantation. The magnetic order of proton-irradiation-induced defects in graphite is investigated with electron spin resonance (ESR) spectroscopy, showing that there is an insulating magnetic region isolating the defect regions of a metallic island inside from the metallic graphite background outside.[18] The origin of ferromagnetism of graphite is unclear, which is also explained with the results of the theoretical calculations. Theoretical studies suggested that ferromagnetism of carbon materials is possible. Vacancies in graphene can introduce quasilocalized states at the Fermi level, leading to a very strong enhancement of local density of states around a vacancy.[19,20] This suggests that vacancies could easily induce local moments in graphene-based systems, and calculations based on the spin-polarized density functional theory (DFT) reveal that vacancies,[21−26] vacancy-hydrogen,[21,24,27−29] hydrogen adsorption defects,[22] adatoms[30] and zigzag edge[31,32] can have net magnetic moment. Vacancies play an important role in the ferromagnetism of graphite, which is revealed by scanning tunneling microscopy (STM) and scanning tunneling spectroscopy (STS).[33,34] C–H bonds and chemisorbed hydrogen also play an important role in the ferromagnetism of graphite, which is revealed by XMCD spectra.[10] Magnetism of graphite can be tuned by $^{12}C^{+}$ ion implantation and H^{+} ion implantation. The $^{12}C^{+}$ ion implantation can introduce vacancies and adatoms in graphite. The H^{+} ion implantation can introduce C–H bonds, hydrogen absorption defects and vacancies. If defects can really induce magnetic ordering, the origin of ferromagnetism of graphite can be investigated with the ESR spectrum, which can be used to study magnetic systems with unpaired electrons and interaction between them.[35−37] In this study, we employ ESR spectra and SQUID magnetometer to study the magnetism of HOPG samples implanted by $^{12}C^{+}$ and H^{+} ions, respectively.

The HOPG samples used in our experiments is ZYA grade (0.4° rocking curve width), from NTMDT Inc. The HOPG samples in dimensions $3\times3\times0.1\,mm^3$ were implanted, respectively, by $^{12}C^{+}$ and H^{+} ions at room temperature. Our previous studies[11] revealed that ferromagnetism of HOPG can be tuned by ion implantation. Ferromagnetism of HOPG induced by 70 keV $^{12}C^{+}$ ion implantation has a maximum at

*Supported by the Research Foundation for Young Scientist in Shandong Province under Grant No BS2013CL043.
**Corresponding author. Email: yangxinmei@sinap.ac.cn
© 2016 Chinese Physical Society and IOP Publishing Ltd

$2 \times 10^{15}\,\mathrm{cm}^{-2}$. Therefore, in the present study, one piece of the HOPG sample was implanted twice with a scanning beam of 70 keV $^{12}C^{+}$ ions to 3×10^{14} and $1 \times 10^{15}\,\mathrm{cm}^{-2}$, respectively. ESR measurements were performed after each implantation step. Five pieces of the HOPG samples were implanted by using a broad H^{+} ion beam with a radius of 0.3 cm at implantation energies of 2.25 MeV, 1.0 MeV, 0.8 MeV, 70 keV, and 15 keV up to 2×10^{17}, 9.2×10^{16}, 6×10^{16}, 2×10^{16}, and $1 \times 10^{16}\,\mathrm{cm}^{-2}$, respectively, to produce almost the same maximum density of defects. A SQUID (Quantum Design) with a sensitivity of $\leq 10^{-7}$ emu was used to measure magnetic moments at room temperature with an applied magnetic field cycling between −1.0 and 1.0 T. A JEOL JES-FA200 spectrometer working at X-band microwave frequency was used to measure the ESR spectra. Proton-induced x-ray emission (PIXE) spectra with a microbeam were used to detect impurities. It is found that Fe content in samples is about 1 μg per gram graphite, and other magnetic metal impurities are below the detection limit of PIXE.

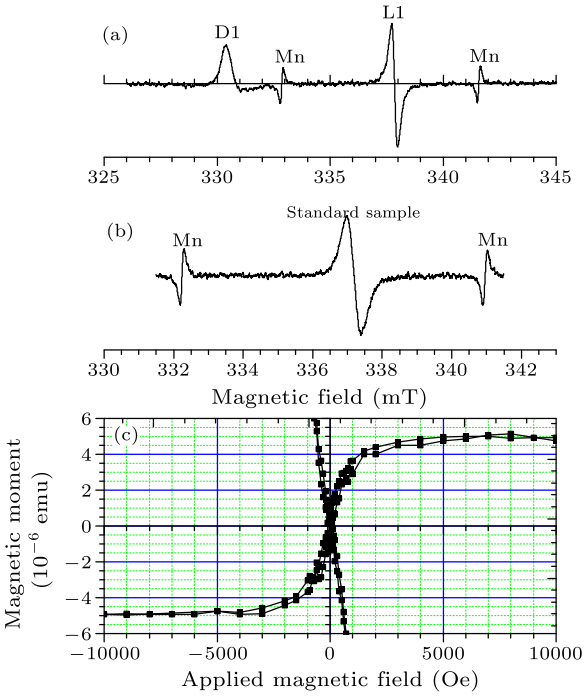

Fig. 1. (Color online) (a) ESR spectra of $^{12}C^{+}$ ion ($1 \times 10^{15}\,\mathrm{cm}^{-2}$) implanted HOPG at room temperature, measured with the Mn marker and with magnetic field applied parallel to the *c*-axis. (b) ESR spectra of the standard sample (2,2,6,6-tetramethylpiperidine-1oxyl) with 6.2631×10^{14} unpaired electrons. (c) The magnetic moment of the same sample as (a), measured at room temperature with the applied magnetic field cycling between −1 T and 1 T.

Our previous studies reveal that the 70 keV $^{12}C^{+}$ ion can produce stable room temperature ferromagnetism in HOPG. The ferromagnetism is increasing with the ion implantation dose from 3×10^{14} to $2 \times 10^{15}\,\mathrm{cm}^{-2}$.[11] Our studies also reveal that the ferromagnetism of HOPG is induced by defects.[12] Therefore, in this study, we combine the ESR spectra with magnetic moment measurements to study the magnetism of the HOPG samples implanted with 70 keV $^{12}C^{+}$ ion at a dose of $1 \times 10^{15}\,\mathrm{cm}^{-2}$. Figure 1(a) is the ESR spectrum of the $^{12}C^{+}$ ion-implanted HOPG sample with the Mn marker, measured with magnetic field parallel to the *c*-axis. There are two resonance lines in this sample, a Dysonian line (D1) and an L1 line. For D1 and L1 lines, the *g* factors are $g_{D1} \sim 2.0447$ and $g_{L1} \sim 2.0023$, which are calibrated by use of the Mn marker. Figure 1(b) is the ESR spectrum of the standard sample with the Mn marker, containing 6.2631×10^{14} unpaired electrons. Comparing the ESR spectra in Figs. 1(a) and 1(b), we find that there are about 1.1318×10^{15} unpaired electrons in the $^{12}C^{+}$ ion-implanted HOPG sample. The unpaired electrons can produce about 5.2483×10^{-6} emu of magnetic moment, which is consistent with the saturated magnetic moment in Fig. 1(c) measured with SQUID.

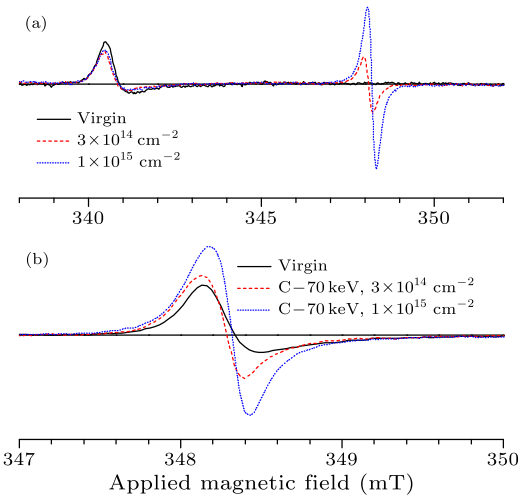

Fig. 2. (Color online) The ESR spectra of the virgin HOPG sample and the 70 keV $^{12}C^{+}$ ion-implanted sample to 3×10^{14} and $1 \times 10^{15}\,\mathrm{cm}^{-2}$, respectively, measured at room temperature: (a) measured with the applied magnetic field parallel to the *c*-axis, and (b) measured with the applied magnetic field perpendicular to the *c*-axis.

Figure 2 is the ESR spectra of the HOPG sample before and after 70 keV $^{12}C^{+}$ ion implantation, which is measured at room temperature. Figure 2(a) is measured with the applied magnetic field parallel to the *c*-axis, showing that $^{12}C^{+}$ ion implantation produces an L1 line at the resonance field close to that of free electrons, and also showing that the implanted HOPG sample has a D1 line at the same resonance field as that of the virgin HOPG sample. The intensity of the D1 line slightly decreases after the first $^{12}C^{+}$ ion implantation and keeps constant upon the second implantation with the same ion at the same implantation energy. Therefore, the D1 line in the implanted sample is ascribed to the conduction carriers[38–40] in the sample beneath the implanted layer. Contrary to the D1 line, intensity of the L1 line increases remarkably with the implantation dose. It is indicated that the L1 line is induced by defects produced by ion implantation. The L1 line (blue) of HOPG implanted with dose of $1.0 \times 10^{15}\,\mathrm{cm}^{-2}$ is slightly asymmetric, while such an asymmetric feature is not observable for the L1 line (red) of HOPG implanted with a dose of $3.0 \times 10^{14}\,\mathrm{cm}^{-2}$. A similar asymmetric L1 line for the 2.25 MeV H^{+} ion im-

planted HOPG sample was also reported,[18] which can be fitted by a sum of a Dysonian component and a small and broad Gaussian one. The asymmetric L1 line in our $^{12}C^{+}$ implanted HOPG sample can be fitted with a Lorentzian component and a small Gaussian one. The thickness of the defective layer induced by 70 keV $^{12}C^{+}$ ion implantation is narrower than the penetration depth of microwave used in ESR measurements, therefore, the ESR signals from both localized spins and conduction carriers in this layer should be symmetric Lorentzian or Gaussian.[41] Since different types of electron spins create an overlapping single L1 line, there are strong interactions among electrons.[42] Therefore, the L1 line of 70 keV $^{12}C^{+}$ ion-implanted HOPG sample (dose: 1.0×10^{15} cm^{-2}) originates from electrons associated with localized defects and conduction electrons. For example, interstitial-vacancy pairs are well-known paramagnetic defects in neutron irradiated graphite.[42] Vacancies have been predicted to induce localized magnetic moments in graphite or graphene[11,12,19–22] and they are closely correlated with the ferromagnetism of graphite.[12,19,20] Interactions between spin-polarized electrons associated with vacancies and implantation induced carriers in π band are likely responsible for the ferromagnetic order of implanted HOPG. This explanation is also consistent with the impurity bands model[46] for ferromagnetism and resonance electron density of states (DOS) around the Fermi level of graphite predicted by DFT calculations.[11] Figure 2(b) is ESR spectrum measured with the applied magnetic field perpendicular to the c-axis of graphite. Although D1 and L1 lines merge together, it clearly shows that the intensity of ESR spectra increases with the implantation dose. It is evidence that the number of unpaired electrons is increased by $^{12}C^{+}$ ion implantation for dose increasing from 3×10^{14} to 1×10^{15} cm^{-2}. The evolution of L1 line intensity with dose shown in Fig. 2(a) is consistent with the evolution of ferromagnetism with $^{12}C^{+}$ ion implantation.[11]

Experiments indicate that there are three peaks in the 2.25 MeV H^{+} ion-implanted HOPG sample.[36] The difference of ESR spectra between 70 keV $^{12}C^{+}$ ion-implanted HOPG and 2.25 MeV H^{+} ion-implanted HOPG may be related to the different spatial distributions of defect density. Therefore, the ESR spectrum of the HOPG sample implanted with 15 keV H^{+} ions is investigated and compared with that of the 70 keV $^{12}C^{+}$ ion-implanted HOPG sample. According to the range and stopping theory as well as the SRIM06 simulation in Fig. 3(a), defects produced by 15 keV H^{+} ions have similar distributions as those produced by 70 keV $^{12}C^{+}$ ions. Figure 3(b) is the ESR spectra of the HOPG sample after 15 keV H^{+} ion implantation up to 1×10^{16} cm^{-2}. In Fig. 3(b), there are also two resonance peaks, i.e., D1 and L1 lines. The g factor of the D1 line in Fig. 3(b) is the same as that of the $^{12}C^{+}$ ion-implanted HOPG sample in Fig. 2(a), and the g factor of the L1 line in Fig. 3(b) is also the same as that in Fig. 2(a). It is indicated that distribution and density of defects in ion implanted HOPG take an essential role in determination of the ESR spectrum. Therefore, the difference of ESR spectra in Figs. 2(a) and 3(b) from in Ref. [36] is certainly caused by the different spatial distributions and densities of defects in ion-implanted graphite, which are closely related to the thickness of the defective layer determined by ion species and energy used during implantation.

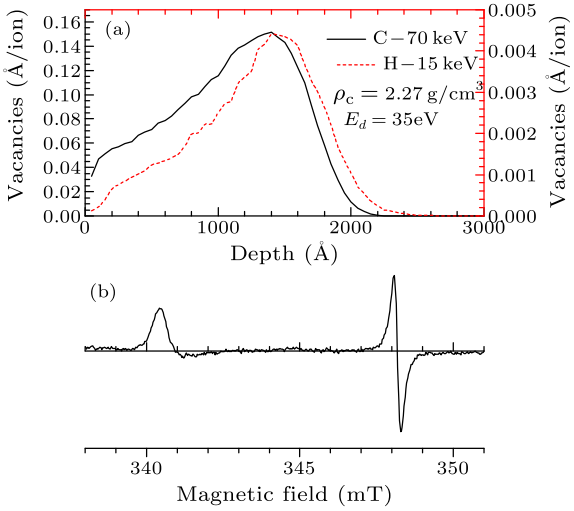

Fig. 3. (Color online) (a) Vacancy density distribution in carbon substrate: the black and the red lines are for 70 keV $^{12}C^{+}$ and 15 keV H^{+} ion implantation, respectively. (b) ESR spectra of HOPG implanted with 15 keV H^{+} ion up to 1×10^{16} cm^{-2}, measured with the applied magnetic field parallel to the c-axis at room temperature.

Figure 4(a) is the ESR spectra of the HOPG samples after H^{+} ion implantation with different energies between 70 keV and 2.25 MeV, measured with the applied magnetic field parallel to the c-axis, showing that there are three resonance lines (D1, D2 and L1) for the implantation energy equal to or higher than 0.8 MeV. The D2 line in Fig. 4(a) has a decreasing g factor with decreasing the ion implantation energy, which indicates that the position of the D2 line induced by ion implantation is related to the implanted energy. Figure 4(b) is the spectra of the HOPG sample after 2.25 MeV H^{+} ion implantation up to 2×10^{17} cm^{-2} (measured at room temperature with the applied magnetic field from the a–b plane to the c-axis and then back to the a–b plane). The D1 line in Fig. 4(b) is a Dysonian line with the same anisotropy as that of the virgin HOPG sample, which indicates that the D1 line is ascribed to the carriers in the HOPG sample beneath the implanted layer (D region in Fig. 4(c)). The D2 line induced by ion implantation is a Dysonian line with a degraded anisotropy of the g factor as compared with the D1 line. It is indicated that the symmetry of crystal in the region responsible for the D2 line is degraded.[35] The D2 line should be attributed to the HOPG sample near the surface (D′ region in Fig. 4(c)) where density of defects is lower and the symmetry of HOPG crystal is degraded. With decreasing the implantation energy, the symmetry of D′ region continuously degrades accompanied by a gradual increase of defect density and g factor lowering (the resonance field shifting to higher value). When the implantation energy reduces to 70 keV, density of defects is high enough to make adjacent defects close enough resulting in electrons trapped on defects. Conduction elec-

trons in this region strongly interact to form a single L1 line.[42] Therefore, the D2 line disappears at this implanted energy. The appearance of the D2 line for implantation energies to be equal to or higher than 0.8 MeV indicates that density of defects in the D′ region decreases with increasing the implantation energy and interactions between electrons associated with localized defects, and conduction electrons are lost. Resonance field of the L1 line and the corresponding g factor are independent of the angle between the c-axis and the applied magnetic field, a character of spins associated with localized defects. The L1 line should be attributed to the defects around the average stopping depth (L region in Fig. 4(c)). Two cases may happen in this region: one is that high density of defects has not destroyed the basic crystal structure, and localized spins can interact with extrinsic carriers induced by doping effect of defects themselves to form magnetic coupling; the second is that defects completely destroyed crystal structure leading to the suppression of magnetic order. Therefore, there is a proper window of defect density, in which ferromagnetic order can readily take place. Outside this window, too small defect density or too large separation between defects result in localized spins not coupling with each other through interactions with irradiation creating extra carriers,[42] and on the other hand, too large defect density can ruin the crystal structure of HOPG to lose magnetic order. Such a defect density window related to the optimized implantation dose have been reported experimentally for proton irradiated HOPG[7] and $^{12}C^{+}$ ion-implanted HOPG.[11] These analyses are further confirmed by the ESR spectra in Fig. 4(d), which are measured at different temperatures. The D1 line in Fig. 4(d) has the same evolution of temperature as that of the virgin HOPG, further confirmed that the D1 line is attributed to carriers in the unaffected part of implanted HOPG, i.e., the HOPG bulk beneath the implanted layer. The behavior of the D1 line can be explained by the evidence of effective internal field in graphite.[43] The effective internal field increases with the decreasing temperature and results in the increase of the g factor of the D1 line.[43] The g factor of the D2 line in Fig. 4(d) slightly increases with the decreasing temperature, suggesting that the mobility of carriers in graphite with lower density of defects is limited. Therefore, there is still anisotropic internal field in the D′ region, which is slightly increasing with the decreasing temperature. Slight increase of line width of D2 with decreasing of temperature indicates that density of defects in the D′ region is very low since defect-induced scattering does not affect line width very much. The g factor of the L1 line in Fig. 4(d) is independent of temperature, thus the L1 line is ascribed to electrons associated with localized defects around average stopping depth (L region schematically shown in Fig. 4(c)). Other evidence to support this ascription is that the intensity of the L1 line decreases with the increasing temperature (the inset of Fig. 4(d)), due to the fact that the density of effective electrons captured by localized defects decreases with temperature. In fact, in addition to paramagnetic defects, magnetic defects such as vacancies can produce localized magnetic moments and substantially modify the electronic states near Fermi energy to induce extra holes in the π band.[42] Theoretical calculation using DFT also predicts that vacancies will induce spin-polarized resonance states at the Fermi level.[11] Therefore, there should be interactions between itinerant electrons and those associated with localized defects to form an asymmetric resonance L1 line. The ferromagnetic order is most likely to be manifested by this line.

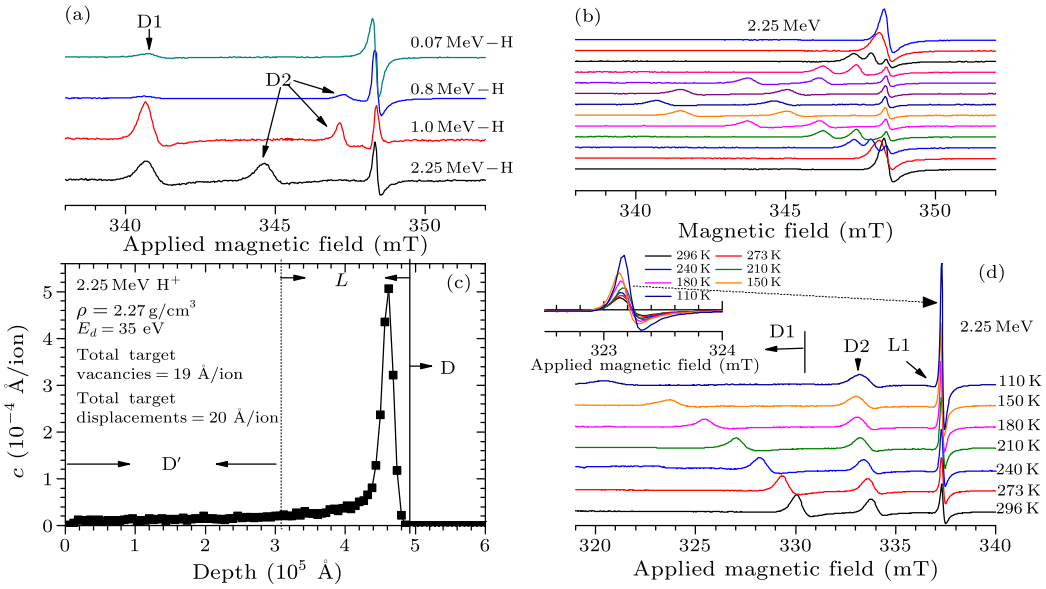

Fig. 4. (Color online) (a) ESR spectra of the HOPG implanted with H^{+} ion (implanted energies are 70 keV, 0.8 MeV, 1.0 MeV and 2.25 MeV, respectively), measured at room temperature with the applied magnetic field parallel to the c-axis. (b) ESR spectra of the HOPG sample implanted by 2.25 MeV H^{+} ion up to 2×10^{17} cm^{-2}, measured at room temperature with the applied magnetic field from the a–b plane to the c-axis and then to the a–b plane. (c) Schematic distribution of vacancies induced by 2.25 MeV H^{+} ions. (d) Temperature evolution of the ESR spectra, measured with the applied magnetic field parallel to the c-axis. The inset in (d) focuses on a part of ESR around the L1 line.

The above results indicate that ferromagnetism of graphite induced by $^{12}C^+$ ion and H^+ ion implantation should be attributed to irradiation produced magnetic defects, such as vacancies including single vacancies and some type of vacancy clusters (multivacancies). Implantation can also produce paramagnetic defects, such as interstitial-vacancy pair defects. Our previous work on magnetic moment measurements at low temperature from 5 to 50 K for the 70 keV $^{12}C^+$ ion-implanted HOPG sample has shown that Curie's law is obeyed very well at low temperature, indicating the Curie paramagnetic behavior. Based on Curie's law, the density of paramagnetic defects is estimated to be in the same order as vacancy density.[39] This is a reasonable result from the viewpoint of defect production by irradiation, since both paramagnetic defects and ferromagnetic defects are governed by the same collisional cascades and subsequential lattice relaxation process. At higher temperature, e.g., room temperature, Curie paramagnetism diminishes, and Pauli paramagnetism of conduction electrons is only in the order of 10^{-8} emu/g.[42] Therefore, the magnetic behavior shown in Fig. 1(c) is mainly contributed by ferromagnetism.

From the above analysis, it is clear that ESR spectroscopy is very useful for understanding the magnetic order in irradiated graphite. However, it needs collaborative studies such as magnetic moment measurements under various conditions,[7,11] soft x-ray absorption spectroscopy,[3] positron spectroscopy,[12] Raman spectroscopy,[39] and detailed spatial profiles of defects induced by the irradiation, etc, to obtain reliably experimental information on ferromagnetic order in this material. Based on the present ESR spectroscopy, it is evident that the number of lines, g factor and line width of each line, and the shape of the L1 line are dependent on ion species, implantation energy and dose. These parameters govern the spatial density distribution of defects produced by irradiation. Density of defects takes an essential role in determination of the magnetism in graphite. For instance, 70 keV $^{12}C^+$ ion-implantation and 15 keV proton implantation produced similar vacancy density distributions in HOPG (Fig. 3(a)), and similar ESR spectra, as shown in Figs. 2(a) and 3(b), respectively. There is a window of defect density (or implantation dose) for ferromagnetic order in 70 keV $^{12}C^+$ implanted HOPG,[11,39] in which the averaged separation between defects is estimated to be in the order of 0.8–2.0 nm. A similar window was also observed in 2.25 MeV proton irradiated HOPG.[7] Therefore, ferromagnetic order in irradiated graphite may exist in a partial region of the whole implantation layer to meet the defect density requirement. For example, the ferromagnetic order may exist in the whole implanted layer for 70 keV $^{12}C^+$ ion-implanted HOPG and for 15 keV proton-implanted HOPG, while it may exist near the end region (L region schematically shown in Fig. 4(c)) of the penetration range of 2.25 MeV proton beam, where the density of vacancies is relatively high to meet the density window.

In summary, we have employed ESR spectroscopy and magnetization measurements associated with H^+ and $^{12}C^+$ ion implantation to study the possible mechanism of magnetic order in energetic ion-irradiated graphite. ESR spectra are related to the spatial distributions of defect density, which can be tuned by ion species, implantation energy and dose. Density of defects in irradiated HOPG is essential for magnetic order. The asymmetric L1 line has character of fixed g factor, and increasing intensity with irradiation dose. Ferromagnetic order likely happens in the region with relatively high density of defects, where magnetic defects such as vacancies may substantially change the electronic structure at Fermi energy causing formation of 'impurity' bands and thus ferromagnetic order.

References

[1] Esquinazi P et al 2002 *Phys. Rev.* B **66** 024429
[2] Esquinazi P et al 2010 *J. Magn. Magn. Mater.* **322** 1156
[3] Ohldag H et al 2007 *Phys. Rev. Lett.* **98** 187204
[4] Han K H et al 2003 *Adv. Mater.* **15** 1719
[5] Esquinazi P et al 2004 *Carbon* **42** 1213
[6] Spemann D et al 2004 *Nucl. Instrum. Methods Phys. Res. Sect.* B **219** 886
[7] Esquinazi P et al 2003 *Phys. Rev. Lett.* **91** 227201
[8] Barzola-Quiquia J et al 2007 *Phys. Rev.* B **76** 161403(R)
[9] Barzola-Quiquia J et al 2007 *Nucl. Instrum. Methods Phys. Res. Sect.* B **256** 412
[10] Ohldag H et al 2010 *New J. Phys.* **12** 123012
[11] Xia H et al 2008 *Adv. Mater.* **20** 4679
[12] Yang X et al 2009 *Carbon* **47** 1399
[13] Barzola-Quiquia J et al 2008 *Eur. Phys. J.* B **61** 127
[14] Levanyuk A P and García N 1992 *J. Phys.: Condens. Matter* **4** 10277
[15] Serena P A et al 1993 *Phys. Rev.* B **47** 5027
[16] Dedkov Yu S and Fonin M 2010 *New J. Phys.* **12** 125004
[17] Schindler K et al 2008 *Phys. Rev.* B **78** 045433
[18] Lee K W et al 2010 *J. Appl. Phys.* **107** 044302
[19] Pereira M V et al 2006 *Phys. Rev. Lett.* **96** 036801
[20] Pereira M V et al 2008 *Phys. Rev.* B **77** 115109
[21] Lehtinen P O et al 2004 *Phys. Rev. Lett.* **93** 187202
[22] Yazyev O V and Helm L 2007 *Phys. Rev.* B **75** 125408
[23] Zhang Y et al 2007 *Phys. Rev. Lett.* **99** 107201
[24] Yazyev O V 2008 *Phys. Rev. Lett.* **101** 037203
[25] Andriotis A N et al 2006 *Phys. Rev.* B **74** 153403
[26] Palacios J J et al 2008 *Phys. Rev.* B **77** 195428
[27] Zhou J et al 2009 *Nano Lett.* **9** 3867
[28] Pisani L et al 2008 *New J. Phys.* **10** 033002
[29] Kusakabe K and Maruyama M 2003 *Phys. Rev.* B **67** 092406
[30] Park N et al 2003 *Phys. Rev. Lett.* **91** 237204
[31] Yazyev V O and Katanelson M I 2008 *Phys. Rev. Lett.* **100** 047209
[32] Son Y et al 2006 *Nature* **444** 347
[33] Ugeda M M et al 2010 *Phys. Rev. Lett.* **104** 096804
[34] Niimi Y et al 2008 *Physica* E **40** 1298
[35] Weil J A and Bolton J R 2007 *Electron Paramagnetic Resonance: Elementary Theory and Practical Applications* (New Jersey: John Wiley Sons) p 36
[36] Lee K W and Lee C E 2006 *Phys. Rev. Lett.* **97** 137206
[37] He Z et al 2011 *Carbon* **49** 1931
[38] Huber D L et al 2004 *Phys. Rev.* B **70** 125417
[39] Wagoner G 1960 *Phys. Rev.* **118** 647
[40] Feher G and Kip A F 1955 *Phys. Rev.* **98** 337
[41] Chipara M et al 2006 *Adv. Mater.* **8** 820
[42] Beuneu F et al 1999 *Phys. Rev.* B **59** 5945
[43] Sercheli M S et al 2002 *Solid State Commun.* **121** 579
[44] Chakhalian J A et al 2002 *Phys. Rev.* B **66** 155107
[45] Lieb E H 1989 *Phys. Rev. Lett.* **62** 1201
[46] Edwards D M and Katsnelson M I 2006 *J. Phys.: Condens. Matter* **18** 7209
[47] Vozmediano M A H et al 2005 *Phys. Rev.* B **72** 155121